EVALUATION OF THE RELATIONSHIP BETWEEN SATURATED HYDRAULIC CONDUCTIVITY AND GRAIN-SIZE DISTRIBUTION OF FLUVIO-GLACIAL DEPOSITS, PUGET LOWLAND, WASHINGTON

Lam Nguyen

A report prepared in partial fulfillment of
the requirements for the degree of

Master of Science
Earth and Space Sciences: Applied Geosciences

University of Washington

December 2013

Project mentor:
Curtis Koger, Associated Earth Sciences, Inc.
Jenny Saltonstall, Associated Earth Sciences, Inc.

Internship coordinator:
Kathy Troost

Reading committee:
Michael Brown
Jody Bourgeois

MESSAGE Technical Report Number: 003

ABSTRACT

The relationship between saturated hydraulic conductivity (*Ks*) and grain-size distribution was evaluated for 49 sites underlain by either glacially over consolidated or normally consolidated fluvio-glacial deposits in the Puget Lowland. A linear regression comprising pairs of grain-size analyses and pilot infiltration tests predicts *Ks* with a 1σ uncertainty of a factor of about 3.5 with 70% of the population variance accounted for. The correlation coefficient R^2 of about 0.90 shows that there is a strong correlation between the grain-size distribution and *Ks*. In contrast, a widely applied analysis proposed by Massmann (2003) explains only 20% of the population variance for normally consolidated materials with an R^2 of only 0.15. That analysis entirely fails to explain the population variance for over consolidated materials. The method developed in this study is recommended for determination of *Ks* for fluvio-glacial deposits of the Puget Lowland.

TABLE OF CONTENTS

List of Figures page

List of Tables page

List of Appendices page

Key to Symbols

A = cross-sectional area perpendicular to flow (l^2)

b_0, b_1, b_2, b_3, and b_4 = model parameters

d_{10}, d_{50}, d_{60}, and d_{90} = grain sizes (mm) where 10, 50, 60, and 90% of material is more fine

f = infiltration rate of water through unit cross-section of porous material (l/t)

f_c = constant-head infiltration rate averaged over last hour of constant-head test (l/t)

f_f = falling-head infiltration rate (l/t)

f_{fines} = fraction of material (by weight) that passes the number-200 sieve (0.075 mm)

$f(t)$ = infiltration rate at time t (l/t)

H_0 = depth of water in pond or infiltration facility (l)

$[H_0 + L_{wf} + h_{wf} / L_{wf}]$ = hydraulic gradient for vertical infiltration (l/l)

Δh = change in hydraulic head (l)

Δh_c = change in head per time step (l)

Δh_f = change in head at beginning and end of falling-head test (l)

$\Delta h/L$ = hydraulic gradient (l/l)

h_{wf} = average capillary head at wetting front (l)

i = short-hand notation for hydraulic gradient (l/l)

i_v = short-hand notation for vertical hydraulic gradient (l/l)

K = hydraulic conductivity (l/t)

Ks = saturated hydraulic conductivity (l/t) (associated with vertical (saturated) flow through the vadose zone)

Ks_f = Ks determined on the basis of field infiltration tests (l/t)

Ks_r = Ks determined from the grain size distribution regression equations (l/t)

L = flow path length (l)

L_{wf} = depth of a sharp wetting front below the bottom of pond (l)

Q = volumetric flow rate (l^3/t)

q = discharge per time step (l/t)

R^2 = correlation coefficient

Δt_c = change in time per time step (t)

Δt_f = duration of falling-head test (t)

σ = one standard deviation (i.e. the width of the normal distribution of deviations that includes 66.7% of the data).

1 INTRODUCTION

1.1 Background

For over 25 years, King County and the Washington State Department of Ecology (Ecology) have provided effective programs to manage stormwater runoff. Impervious surfaces such as roads, parking lots, and sidewalks prevent rain from infiltrating the ground (Clark, 2009). As a result, stormwater flows over the surface as runoff, causing floods, reducing groundwater recharge, eroding river banks, and delivering pollutants to streams and rivers. Low impact developments (LID) such as rain gardens, below-pavement infiltration systems, and other LID features are designed to capture and retain runoff, thereby reducing the hydrologic impacts to land and resources (King, 2013; Ecology, 2012). To appropriately design LID, there is a need for clearly understanding how the infiltration rate is controlled by the saturated hydraulic conductivity (*Ks*) of materials beneath the LID facilities.

Massmann (2003) recommended field (in-situ) infiltration tests or grain-size analyses, as a basis to estimate *Ks*, to determine LID design features. Although, infiltration tests are the preferred method to determine *Ks*, they are time consuming, require large volumes of water (Massmann, 2003), and can be an order of magnitude more expensive than grain-size analyses (Jenny Saltonstall, Associated Earth Sciences, Inc., personal communication, 2013). However, reliance on grain-size analysis alone has proven problematic since important site-specific characteristics including heterogeneity (Massmann, 2003), the degree of glacial over consolidation (Curtis Koger, Associated Earth Sciences, Inc., personal communication, 2013), and anthropogenic disturbances (Ecology, 2013) may also affect infiltration rates.

Massmann (2003) provided a grain-size-distribution-based method to estimate *Ks* for normally consolidated materials typical of western Washington. However, field infiltration data obtained by AESI indicates that this method fails to adequately determine *Ks* by a full order of magnitude (Curtis Koger, Associated Earth Sciences, Inc., personal communication, 2013). Thus, a need exists to re-evaluate the methodology and calibration of the grain-size estimate for *Ks*.

1.2 Scope of Work

The purpose of this study was to evaluate the relationship between *Ks* and grain-size distribution of fluvio-glacial deposits of the Puget Lowland. The objectives in this study were: (1) to quantify limitations for the method proposed by Massmann (2003); (2) to better predict *Ks* on the basis of a new calibration using grain-size analyses and pilot infiltration tests of fluvio-glacial deposits of the Puget Lowland; and (3) to provide a new recommendation for determining *Ks* and its estimated uncertainty on the basis of site specific information including the local grain-size distribution and the local geologic units. The form of the linear regression analysis performed in this study was motivated by the grain-size components previously identified by Massmann (2003).

1.3 Glacial History

Below is a slightly modified summary of the Puget Lowland's glacial history from Booth and Troost (2005).

The majority of the Puget Lowland is an elongated structural basin between the Cascade Range and the Olympic Mountains. The Puget Lowland has been glaciated repeatedly during the past two million years by coalescing continental glaciers which advanced south from British Columbia. At least seven invasions of glacial ice and alternating non-glacial intervals have left a discontinuous geologic record in the Puget Lowland. The last glacier reached the central Puget Lowland about 15,000 years ago. The Puget Lowland sits atop a complex and incomplete succession of interleaved glacial and non-glacial deposits that overlie an irregular bedrock surface. These glacial and non-glacial deposits vary laterally in both texture and thickness, and they contain many local unconformities.

The topography of the Puget Lowland is dominated by rolling surfaces of mainly sand and till that were deposited during the last ice advance, the Vashon Stade of the Fraser Glaciation. During each successive glaciation, the ice advanced into the lowland as a broad tongue, named the Puget Lobe. At its maximum, the ice was more than 6000 feet thick near Bellingham, 3000 feet thick near Seattle, and about 1800 feet thick southeast of Tacoma (Easterbrook, 2003).

Of the most recent glaciation, variation in depositional environments yielded distinctly different fluvio-glacial deposits. As the ice advanced, streams exiting the front of the ice deposited sand and gravel. These advance outwash deposits (Qva) are generally dense to very dense (i.e. glacially over consolidated), a result of being over-ridden by the thick advancing ice. Streams emanating from the retreating ice also deposited sand and gravel. These recessional outwash deposits (Qvr) however, not over-ridden by ice, are loose to medium dense (normally consolidated). Post-glacial alluvium (Qal), deposited by streams and running water, comprises loose to medium-dense sand, silt, gravel, and cobbles.

2 EQUATIONS

2.1 Darcy's Law and the Green-Ampt Approximation

As reviewed by Massmann (2003), the infiltration rate is controlled by the hydraulic conductivity and the hydraulic gradient under Darcy's Law (Equation 1):

(1) $$f = \frac{Q}{A} = -K\left(\frac{\Delta h}{L}\right) = -Ki$$

where f is the infiltration rate of water through a unit cross-section of a porous material (l/t), Q is the volumetric flow rate (l^3/t), A is the cross-sectional area perpendicular to flow (l^2), K is the hydraulic conductivity (l/t), Δh is the change in hydraulic head (l), L is the flow path length (l), $\Delta h/L$ is the hydraulic gradient (l/l), and i is a short-hand notation for the hydraulic gradient (l/l).

In the case of vertical infiltration through the vadose zone (the shallow unsaturated region), hydraulic conductivity (K) is represented by the saturated hydraulic conductivity (Ks). It is assumed that within the locally saturated zone below a LID installation, Darcy's Law can be used to describe the flow through the Green-Ampt approximation (Equation 2):

(2) $$f(t) = Ks\left[\frac{H_0 + L_{wf} + h_{wf}}{L_{wf}}\right] = Ksi_v$$

where $f(t)$ is the infiltration rate at time t (l/t), Ks is the saturated hydraulic conductivity (l/t), H_0 is the depth of water in the pond or infiltration facility (l), L_{wf} is the depth of a sharp wetting front below the bottom of the pond (l), h_{wf} is the average capillary head at the wetting front (l), and [$H_0 + L_{wf} + h_{wf} / L_{wf}$] is the hydraulic gradient for vertical infiltration, i_v (l/l).

The infiltration rate as a function of time under the Green-Ampt approximation is illustrated in Figure 1. In early time, the infiltration rate is large because the hydraulic gradient is greater than 1.0 (L is small compared to H_0 and h_{wf}). As more water infiltrates, the late-time infiltration rate approaches Ks because the hydraulic gradient approaches 1.0 (L is very large compared to H_0 and h_{wf}). Thus, "short-term" infiltration tests over-estimate the "long-term" infiltration rate.

Once the wetting front reaches a regional or perched water table, the Green-Ampt approximation is no longer valid. Under these conditions, groundwater mounding and lateral infiltration develops. Although the infiltration rate can still be described with Darcy's Law, the gradient term is much more difficult to quantify or predict. Thus, appropriate estimates of Ks should be measured under near steady-state (the "long-term" infiltration rate) and vertical infiltration conditions with care to avoid measurement after the wetting front has reached the local water table.

2.2 Relationship between Grain-Size Distribution and Hydraulic Conductivity

Grain-size analysis measures size distribution of grains (grain-size distribution) based on their capacity to pass through sieves of various mesh sizes. Grain-size distribution provides information on grain characteristics including averaged grain-size diameters and degree of sorting. Hydraulic conductivity (K) is related to permeability (properties of the porous medium) and a manifestation of grain-size distribution. For well-sorted sediments, permeability is proportional to square of the grain-size diameter. Permeability increases for coarser grains due to larger pore openings while permeability decreases for finer grains due to increase frictional resistance to flow from the porous medium. Permeability also decreases for poorly-sorted sediments, where finer grains fill the voids within the porous medium. For normally consolidated sediments, K of well-sorted sands is typically between 10^1 and 10^2 inches per hour (iph) whereas

for poorly-sorted sands (silty sands and fine sands), K is typically between 10^{-2} and 10^{1} iph (Fetter, 2001).

For over a century, geologists have explored the relationship between hydraulic conductivity measured in laboratory permeameters and grain-size distributions. In 1911, Hazen observed that K increases as the square of the *effective grain-size diameter* (d_{10}), grain sizes (mm) for which 10% of grains are more fine. Krumbein and Monk (1942) estimated K from the *mean grain size diameter* (d_{50}), grain sizes (mm) for which 50% of grains are more fine, and standard deviation of the complete grain-size distribution. Shepherd (1989) noted that K increases as the i-th power of d_{50} (Fetter, 2001; Massmann, 2003). Alyamani and Sen (1993) used the slope of the grain-size distribution curve between d_{50} and d_{10} to determine K. Rogiers et al. (2012) estimated K by incorporating the complete grain-size distribution in their regression analysis.

The quantitative approach proposed by Massmann (2003) is of particular interest because of its extensive application in the Puget Lowland. Massmann collected samples of natural (normally consolidated) and synthetic materials comprising relatively coarse-grained sands to silty sands. The natural materials were selected from 15 infiltration ponds in western Washington while the synthetic materials were a mixture of silica sand with grain diameters of 1.20 millimeters (mm) (#16 U.S. standard sieve number), 0.30 mm (#50), 0.125 mm (#125), and rock flour (fines). K for each sample was derived from a stand-alone air permeameter test, in which Massmann and Johnson (2001) converted air conductivity to K. *The* grain-size distributions from the natural and synthetic materials and the laboratory determination of K were linearly regressed, giving Equation 3:

$$log_{10}(K) = -1.57 + 1.90d_{10} + 0.015d_{60} - 0.013d_{90} - 2.08f_{fines} \quad (3)$$

where K is the hydraulic conductivity (cm/s), d_{10}, d_{60}, and d_{90} are the grain sizes (mm) for which 10, 60 , and 90% of the material is more fine, and f_{fines} is the fraction of the material (by weight) that passes the number-200 sieve (0.075 mm).

3 METHODS

3.1 Summary

Field infiltration rates and grain-size distributions were analyzed from 19 metropolitan regions throughout the Puget Lowland (Figure 2). In contrast to all previous studies, in this work, values for the saturated hydraulic conductivity (*Ks)* were based on field determinations of infiltration rates rather than being an indirect determination based on disturbed materials studied in the laboratory. A total of 331 grain-size and 133 field-*Ks* data were compiled from AESI's geotechnical reports between the years 2003 to 2013. Within these data, 49 pairs were identified where grain-size measurements and field-*Ks* determinations came from the same infiltration pits (Appendix A). Each grain-size sample was assigned by AESI staff to a geologic unit based on the known map extent and results from visual classification. The following procedures for grain-size analysis and pilot infiltration test are described in detail by AESI (2013), and slightly modified as described in this report.

3.2 Grain-Size Analysis

Soil samples recovered from the field, at the time of drilling/excavation, were brought back to AESI's laboratory for further visual classification and comparison using a system based on the *American Society for Testing and Materials* (ASTM): D-2488, "Standard Practice for Description and Identification of Soils" in conjunction with the Unified Soil Classification System (USCS). Mechanical grain-size analysis was performed on selected soil samples obtained from field testing in general accordance with ASTM: D-422, "Standard Method for Particle-Size Analysis of Soils".

The laboratory testing data were recorded in a spread sheet. A linear interpolation method was used to obtain values for grain-size components used for linear regression and for plotting grain-size distribution curves.

3.3 Pilot Infiltration Test

The infiltration analysis was conducted as a basis of estimating the field-*Ks* (long-term infiltration rate). The infiltration data were measured in an open pit test using the general

methodology described as the pilot infiltration test (PIT). The PIT was modified into a small-scale PIT by AESI, to reduce the cost of the test but still retain reliable information on the infiltration rate. The large-scale and small-scale PITs are referenced in the *Stormwater Management Manual for Western Washington* (SMWW), from Ecology (2012). The following is a detailed description of the small-scale PIT.

An open pit, with a base of 12-32 square-feet, was excavated to a depth that corresponded to the proposed infiltration facility subgrade. In some cases, instead of an open pit, a 28 square-feet infiltrometer (a 6-foot diameter steel ring) was used. The first phase of testing (constant-head phase) began by introducing water through an electronic flow meter with instantaneous flow rate and total flow volume readouts. The water level in the infiltration pits was measured with a staff gauge with a 0.01-foot division.

Water was allowed to rise in the pit until the water level reached approximately 6 to 9 inches above the bottom of the pit. A low head (or height) of water within the pit minimizes sidewall caving (changes in storage) and horizontal infiltration during testing. After the water level reached the target level, the inflow rate was reduced in order to maintain a constant water level (constant-head).

Readings of the water level, instantaneous flow rate, and total flow volume were recorded at approximately 15-minute intervals. The inflow was maintained for a minimum of 6 hours. The constant-head was calculated using Equation 4:

(4) $$f_c = q - [\Delta h_c / \Delta t_c]$$

where f_c is the constant-head infiltration rate (l/t) averaged over the last hour of the constant-head test, q is the discharge (l/t) per time step, derived from the instantaneous flow rate and the test-cell dimension, Δh_c is the change in head per time step (l), and Δt_c is the change in time per time step (t). Here, the early-time infiltration rate (within the first hour) generally deviated from the Green-Ampt approximation. The early-time variation appeared to be a result of adjusting the flow rate during maintenance of a constant-head, after which the infiltration rate achieved near

steady-state behavior. The infiltration rate averaged over the last hour of the constant-head test appeared to be a good approximation of the long-term infiltration rate (*Ks*).

The second phase of testing (falling-head phase) began by discontinuing the water flow immediately after the constant-head phase. After discontinuing the water flow, water levels were measured between one- to five-minute intervals, depending on the infiltration rate. The falling head test was terminated when the head reached zero, normally within an hour or less. The falling-head was calculated using Equation 5:

(5) $$f_f = \Delta h_f / \Delta t_f$$

where f_f is the falling-head infiltration rate (l/t), Δh_f is the change in head at the beginning and end of the falling-head test (l), and Δt_f is the duration of the falling-head test (t). The falling-head infiltration rate was generally within 10% of the constant-head infiltration rate. The falling-head infiltration rate was difficult to measure in more permeable material due to a rapid change in head thus, only the constant-head infiltration rate was used in this study.

Upon completion of the infiltration test, the pits were over-excavated in order to document the types of soils the water infiltrated through. The typical over-excavated depth was between 12 and 15 feet.

Field-*Ks* reported as 0 iph were adjusted to the lowest detectable rate of 0.02 iph which was calculated based on the precision of the staff gauge (0.01 foot) divided by the maximum duration of the constant head test (6 hours).

3.4 Regression Analysis

A best-fit (least-squares) linear regression was performed in Excel based on standard methodology described by Bevington and Robinson (2003). The fitting function is depicted by Equation 6:

(6) $$log_{10}(Ks) = b_0 + b_1 d_{10} + b_2 d_{60} + b_3 d_{90} + b_4 f_{fines}$$

where b_0, b_1, b_2, b_3, and b_4 are the model parameters and the grain-size components are those identified by Massmann (2003) (the log form of *K* is commonly applied in similar applications). Here the convention is adopted to refer to infiltration-based *Ks* as Ks_f while *Ks* predicted from regression equations are given as Ks_r.

Regression equations were derived from the following data sets: (1) Qva or over consolidated material; (2) Qvr+Qal or normally consolidated material; and (3) Qva+Qvr+Qal or mixed materials.

A table of the analysis of variance (ANOVA) is generated after each regression. From the ANOVA, a probability value (p-value) greater than 0.05 (5%) generally suggests a weak correlation between the associated grain-size component and the predicted value (Hooper, 2013). Where p-values were greater than 5%, the associated grain-size component were removed, and another equation was regressed from the reduced set of grain-size components.

A correlation coefficient, R^2 (y-intercept set at 0) and variances were presented for a goodness-of-fit comparison between the observed and predicted data. Variances were calculated for the population (Ks_f) and from the regression predictions (the standard deviation, σ, is given by the square root of the variance). Because *Ks* values frequently vary by more than two orders of magnitude (Fetter, 2001), it is more appropriate to represent the following statistical values in logarithmic space ($\log_{10}(Ks)$). As such, for a predicted *Ks* of 10 iph, a σ of 1 log unit gives the 66.7% confidence interval ranging from 1 to 100 iph (σ in log units is a multiplicative factor).

The arithmetic mean (average) of *Ks* tends to give more weight to the more permeable values. To reduce the effects of this weighting, it is commonly accepted that a more representative description of *Ks* is a log-transformation of the average – the geometric mean (Fetter, 2001). This study presents only the geometric mean.

A grain-size distribution curve of averaged and individual grain-size samples is shown in Figure 3 (data in Appendix B). Averages of Ks_f are shown in Table 1. Tables 2 to 3 summarize the regression analyses. Graphs of the observed against the predicted *Ks* are shown in Figures 4

through 11, from which the solid correlation line ($Ks_f = Ks_r$) and the dotted order of magnitude lines are used for a visual goodness-of-fit comparison (as shown below a factor of 10 is the approximate 95% confidence interval for these data). An open-square data point represents the lowest detectable Ks_f of 0.02 iph. Tabulated regression data are shown in Appendix C to G.

3.5 Uncertainty

Uncertainties that may affect this analysis are summarized here.

- A 10 to 25% measurement error is estimated for the infiltration test. Measurement uncertainties are associated with (1) observed scatter in the last hour constant-head infiltration rate measurements (the last hour measurements were averaged) (2) measurement of the test-pit dimensions, and (3) possible miscalibration or misreading of the flow meter. Higher measurement error is estimated for tests with lower flow-rates and/or smaller pit dimensions and a lower measurement error is estimated for tests with higher flow-rate and/or larger pit dimensions (Jenny Saltonstall, Associated Earth Sciences, Inc., personal communication, 2013).
- A 1% measurement error is estimated for the mechanical grain-size analysis. This uncertainty is associated with the potential loss of sediments (fines) during the sieving process (Eric Knoedler, University of Washington, personal communication, 2013).
- Grain-size distributions may not fully characterize heterogeneous materials beneath the infiltration pit that may include stratified layers of silt and clay. In addition, the grain-size distribution does not characterize microstructures within sedimentary deposits. Small scale cross-stratification could provide high conductivity paths through the material. These macro- to micro-scale structures are potentially sources of large differences in *Ks*.

4 RESULTS & DISCUSSION

4.1 Characteristics of Materials

While the spread of grain-size distribution curves for the individual (Qva, Qvr, and Qal) samples is relatively large, the averaged grain-size distribution curves for over consolidated and normally consolidated materials appear similar (Figure 3). However, the geometric mean Ks_f for the normally consolidated material (17 iph) is 5 times larger than the geometric mean Ks_f for the

over consolidated material (3 iph) (Table 1). Over consolidation within the material results in microstructural differences, reducing permeability. This provides further justification that over consolidated and normally consolidated materials should be analyzed separately

Using Equation A.1 for the over consolidated material (Table 3), about 70% of the population variance is accounted for (the variance of the population of 0.93 is reduced to 0.28). The R^2 of 0.78 shows a good correlation between grain-size distribution and *Ks*. The 1σ of this fit gives a confidence interval for *Ks* prediction of a factor of 3.4. At the 95% confidence level, the confidence interval factor is about 10. As shown in Figure 5, the data follow the correlation line of $Ks_f = Ks_r$ and most of the data lie within the calculated uncertainty bounds.

The variance reduction based on Equation A.2 (Table 3) is similar to Equation A.1 (although it is noteworthy that the R^2, 0.85, is larger). Since this fit contains no details of the coarse distribution ($>d_{10}$), the fine distribution alone determines the permeability of over consolidated materials. This result can be rationalized on the basis of the glacial over consolidation process. In a material with a range of grain sizes, as pore spaces are reduced by compaction, fines are increasingly capable of blocking opening of interconnected pores (pore-throats).

Equation 3 (Massmann 2003) over-predicts *Ks* for the over consolidated material by up to two orders of magnitude (Figure 4). Although the R^2 is 0.68 (Table 3) (suggesting a weak correlation between the grain size distribution and Ks_f), there is no variance reduction from the parent population. It is not surprising that Equation 3 fails to predict *Ks* because the indirect analysis that underlies the equation was not informed by in-situ properties (microstructures) of the over consolidated material.

Using Equation B.1 for the normally consolidated material (Table 3 and Figure 8), 70% of the population variance is accounted for. The R^2 of 0.90 shows a strong correlation between grain-size distribution and *Ks*. The 1σ of this fit gives a confidence interval for the *Ks* prediction of a factor of 3.6. In contrast, Equation 3 (Figure 7) accounts for only 20% of the population variance and the R^2 of 0.12 suggests a poor correlation between grain-size distributions and *Ks*.

The *Ks* predictions for the mixed data sets using Equations C.1 and C.2 are relatively poor. The variance reduction in the parent population is moderate (50%) and the R^2 is small (0.20). These results clearly demonstrate a need to keep predictions of *Ks* separate for over consolidated and normally consolidated materials.

4.2 Recommendations

Based on the analyses and discussions in the previous sections, the following recommendations are made for determining *Ks*.

- The recommended approach in determining *Ks* is through field (in-situ) infiltration tests.
- In the case where the grain-size-distribution-based approach is the only option, the following is recommended for determining *Ks*.
    - A distinction should be made between glacially over consolidated (Qva) and normally consolidated (Qvr+Qal) materials.
    - For Qva, Equations A.1 or A.2 is recommended for determining *Ks*.
    - For Qvr or Qal, Equation B.1 is recommended for determining *Ks*.
    - The recommended determination of *Ks* should be considered as a factor of about 3.5 approximation at a 66.7% confidence interval or a factor of about 10 at a 95% confidence interval.
    - If vertical site variability (inclusion of silt and clay layer) is observed, the effects of groundwater mounding on infiltration performance should be evaluated through hydrologic methods which could include groundwater model, field infiltration testing, and additional grain-size distribution using methods described in the *Stormwater Management Manual for Western Washington* (Ecology, 2012).

4.3 Limitations

The following are limitations in the analyses and recommendations of this study.

- Determination of *Ks* from field infiltration tests is based on the assumption of vertical infiltration through homogeneous material as described by the Green-Ampt approximation (Equation 2).
- Grain-size distributions are assumed to be representative of homogeneous materials. Macro- and micro-scale structures of *in-situ* materials were not characterized.

- The recommended grain-size-based approach for *Ks* has an uncertainty of a factor of about 3.5 at the 66.7% confidence level (or a factor of about 10 at the 95% confidence level).
- The grain-size based approach for determining *Ks* and its estimated uncertainty are applicable for local geologic units identified in this study.
- Equations A.1, A.2 and B.1 were regressed based on a modest sample size (~25).

5 CONCLUSION

For over a century, geologists have explored the relationship between saturated hydraulic conductivity (*Ks*) measured in laboratory permeameters and grain-size distributions. However, results from this study show that data comprising in-situ material properties is needed to better correlate *Ks* and grain-size distribution. Therefore, a relationship between *Ks* and grain-size distribution was evaluated for 49 sites underlain by either glacially over consolidated or normally consolidated fluvio-glacial deposits in the Puget Lowland. Using linear regression, comprising pairs of grain-size analyses and pilot infiltration tests, *Ks* predictions had a 1σ uncertainty of a factor of about 3.5 with 70% of the population variance accounted for. In addition, the R^2 of about 0.90 showed a strong correlation between *Ks* and grain-size distribution. In contrast, a widely applied indirect analysis proposed by Massmann (2003) explained only 20% of the population variance for normally consolidated materials with an R^2 of 0.15 and failed to explain the population variance for over consolidated materials. The method developed in this study is recommended for determination of *Ks* for fluvio-glacial deposits of the Puget Lowland.

6 REFERENCES

AESI, 2013, Hydrogeological and Geotechnical Report, Ballard Natural Drainage Systems 2013 Options Analysis, Seattle Washington: Associated Earth Sciences, Inc., Proj. No. KH130125A, July 9, 2013.

Alyamani, M. S., and Sen, Z., 1993, Determination of Hydraulic Conductivity from Complete Grain-Size Distribution Curves: Ground Water, Vol. 31, No. 4.

Bevington, P. R., and Robinson, D. K., 2003, Data Reduction and Error Analysis for the Physical Sciences, 3rd edition: McGraw-Hill, New York, New York, ch. 7, p. 117-122.

Booth, B. D., and Troost, K. G., 2005, Geologic Map of the Northwestern Seattle area, Washington: The Geological Society of America Reviews in Engineering Geology, Vol. XX, p. 1-35.

Clark, 2009, Stormwater Manual: Clark County, p. 1-4 – 1-6.

Ecology, 2012, 2012 Stormwater Management Manual for Western Washington Volume III: Washington State Department of Ecology, p. 3-65 – 3-102, No. 12-10-030.

Ecology, 2013, Easter Washington Low Impact Development Guidance Manual: Washington State Department of Ecology, Appendix B, p. 169.

Easterbrook, D. J., 2003, Quaternary Geology of the United Stats: INQUA 2003 Field Guide Volume: The Geologic Society of America, p. 22.

Fetter, C. W., 2001, Applied Hydrogeology, 4th edition: Prentice-Hall, Inc., Upper Saddle River, New Jersey, ch. 3, p. 69-88.

Hooper, P., 2013, Mathematical and Statistical Sciences, University of Alberta. Retrieved on November 3, 2013 from: http://www.stat.ualberta.ca/~hooper/teaching/misc/Pvalue.pdf

King, 2013, Stormwater Management Program: King County Department of Natural Resources And Parks and Water and Land Resources Division, p. 7.

Massmann, J. W., 2003, Implementation of Infiltration Ponds Research: Washington State Department of Transportation and United States Department of Transportation.

Massmann, J. W., and Johnson, L., 2001, Applying groundwater flow models in vapor extraction system design: Ground Water, Vol. 34(4), p. 499-503.

NGS, 2013, MapMaker 1-Page Maps: National Geographic Society. Retrieved on October 21, 2013 from: http://education.nationalgeographic.com/education/mapping/outline-map/?map=Washington&ar_a=1

Olanrewaju, J., and Wong, T., 2010, Hydraulic Conductivity, Porosity and Particle Size Distribution of Core Samples of the Upper Glacial Aquifer: Laboratory Observations: Department of Earth and Space Sciences, State University of New York, Stony Brook, NY. Retrieved on November 10, 2013 from: http://dspace.sunyconnect.suny.edu/bitstream/handle/1951/48010/ORLANRE00.pdf?sequence=1

Rogiers, B., Mallants, D., Batelaan, O., Gedeon, M., Huysmans, M., and Dassargues, A., 2012, Estimation of Hydraulic Conductivity and Its Uncertainty from Grain-Size Data Using GLUE and Artificial Neural Networks: Math Geosci, 44:739-763.

Figures

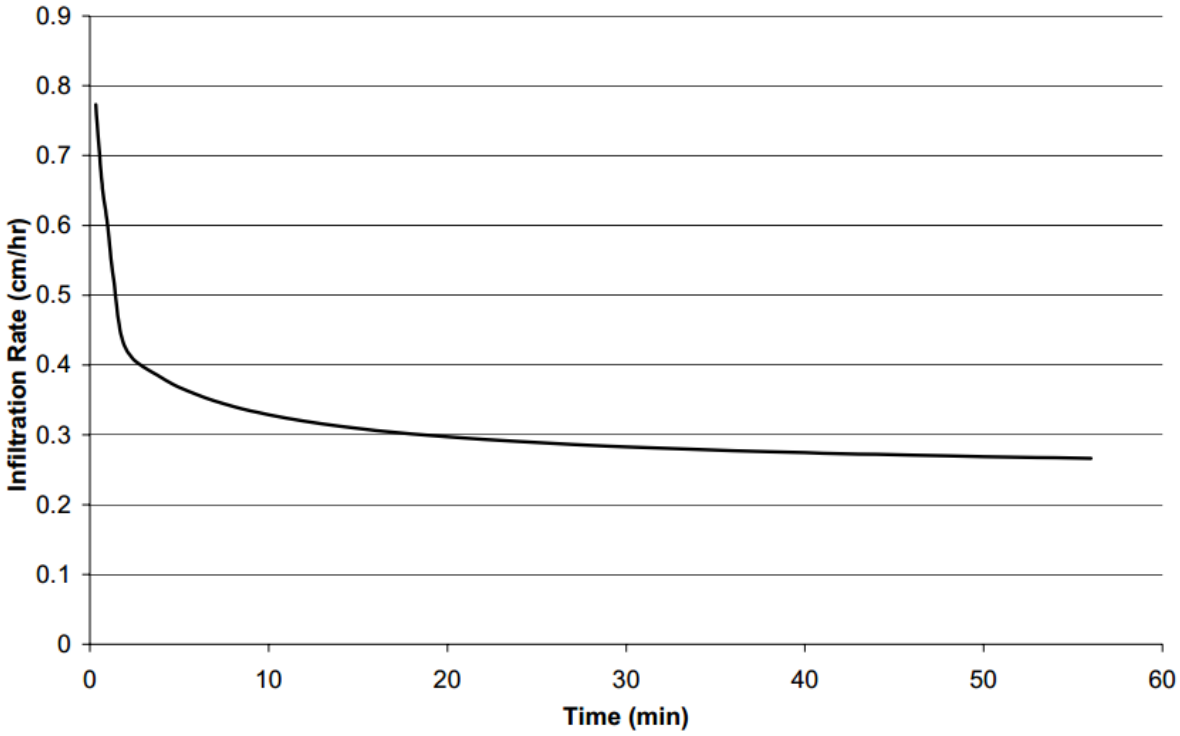

Figure 1. Estimated infiltration rate for loamy sand using the Green-Ampt approximation (Massmann, 2003).

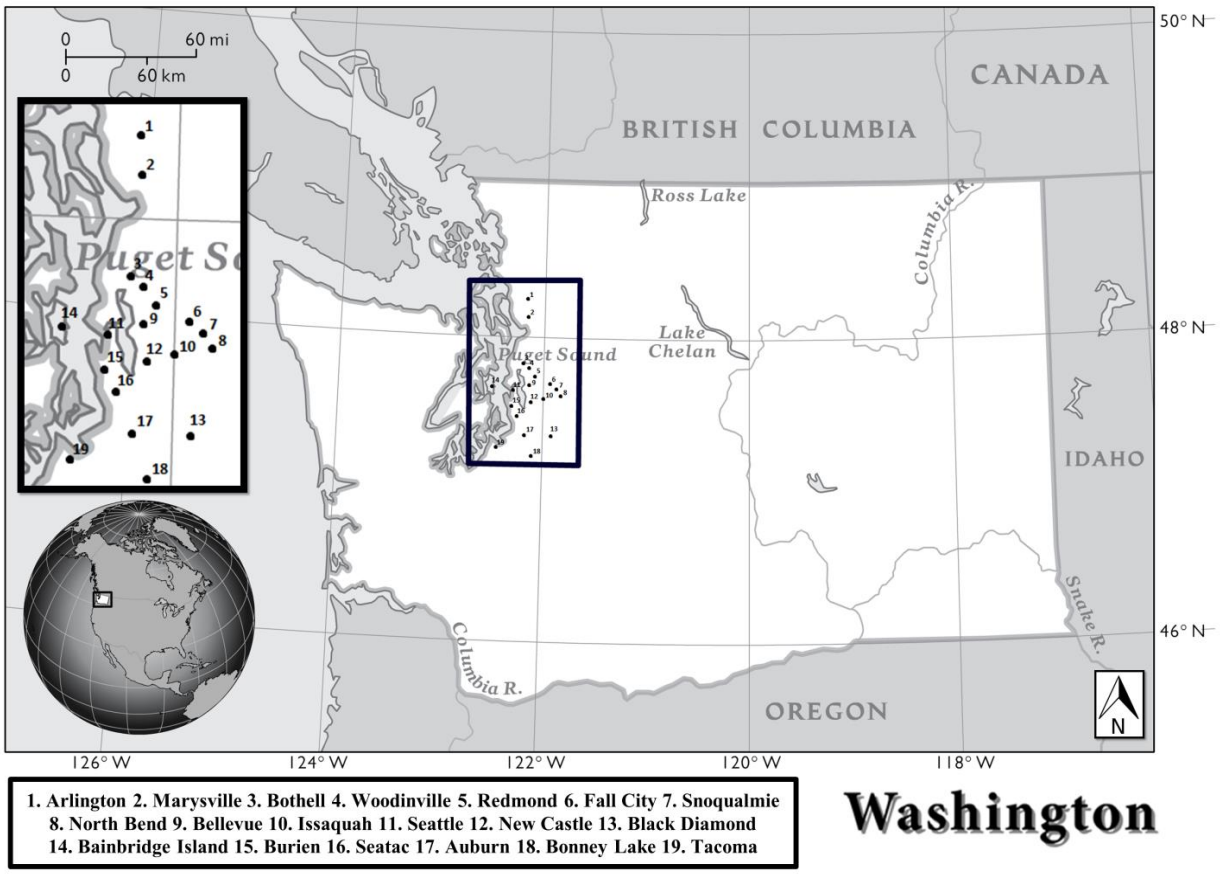

Figure 2. Metropolitan regions where grain-size and field-*Ks* data were obtained. Modified from the National Geographic Society (NGS, 2013).

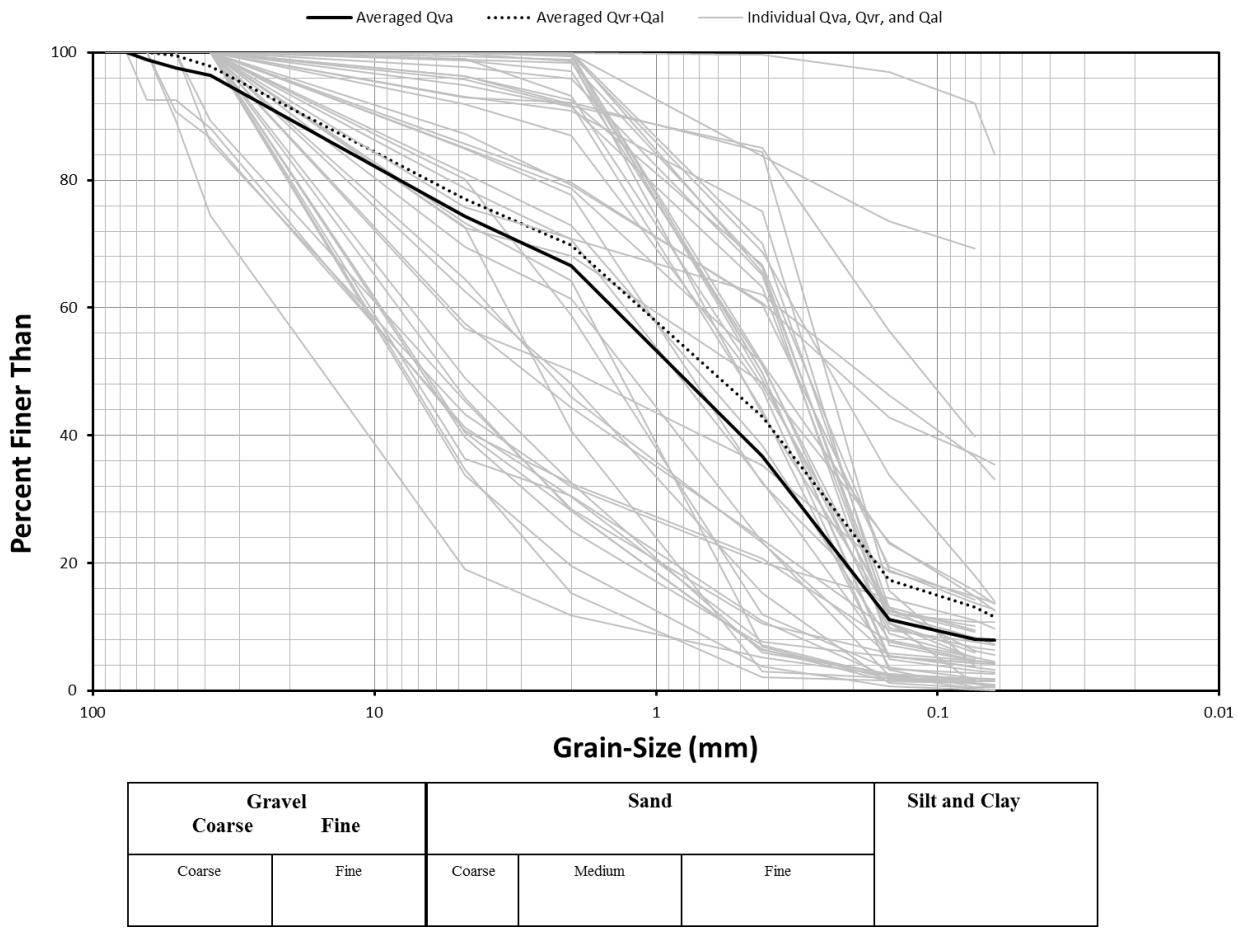

Figure 3. Grain-size distribution curve for averaged over consolidated (Qva) and averaged normally consolidated (Qvr+Qal) samples compared with individual (Qva, Qvr, and Qal) samples. Data shown in Appendix B.

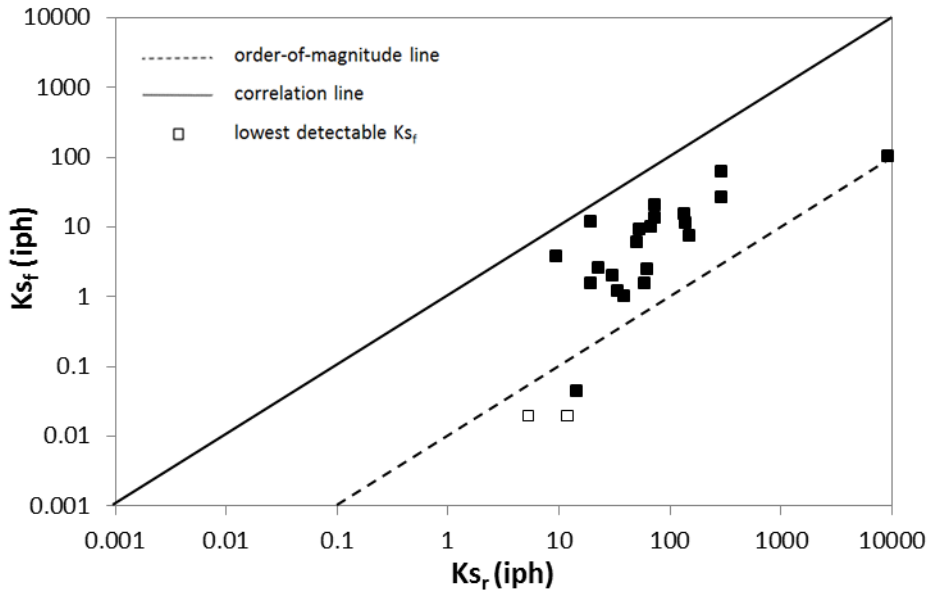

Figure 4. Equation 3 for over consolidated samples (Qva). Ks_f = field saturated hydraulic conductivity (iph) and Ks_r = saturated hydraulic conductivity from regression equations (iph).

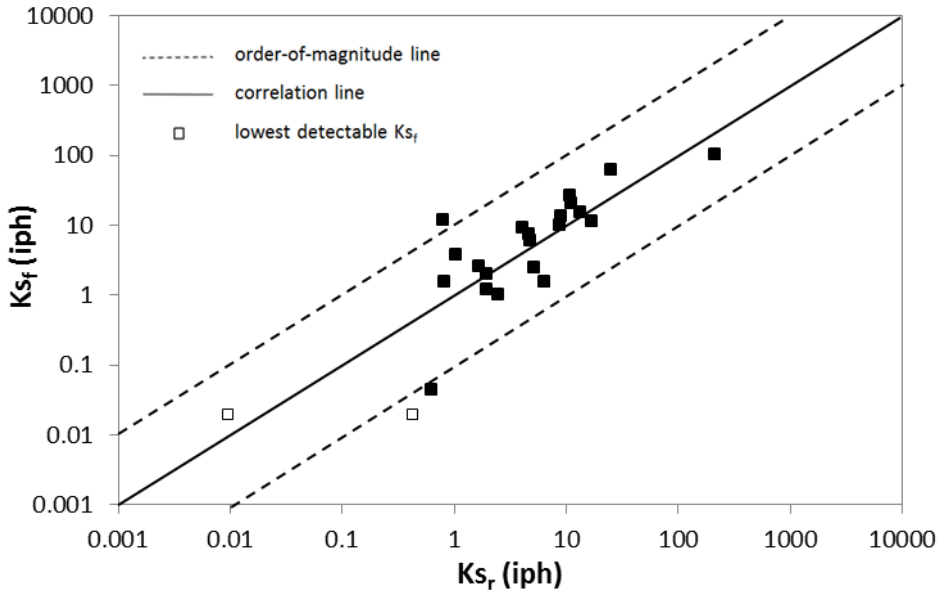

Figure 5. Equation A.1 for over consolidated samples (Qva). Ks_f = field saturated hydraulic conductivity (iph) and Ks_r = saturated hydraulic conductivity from regression equations (iph).

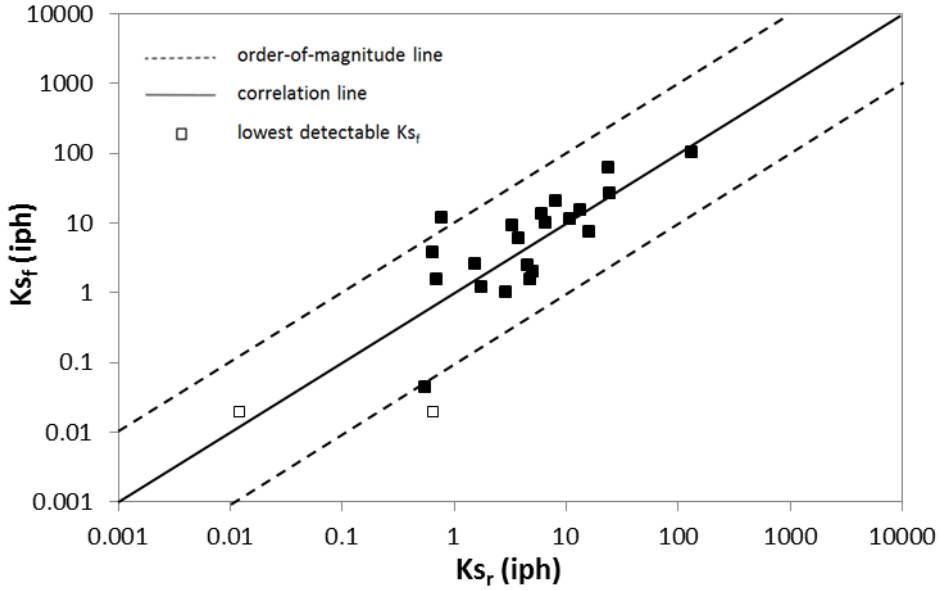

Figure 6. Equation A.2 for over consolidated samples (Qva). Ks_f = field saturated hydraulic conductivity (iph) and Ks_r = saturated hydraulic conductivity from regression equations (iph).

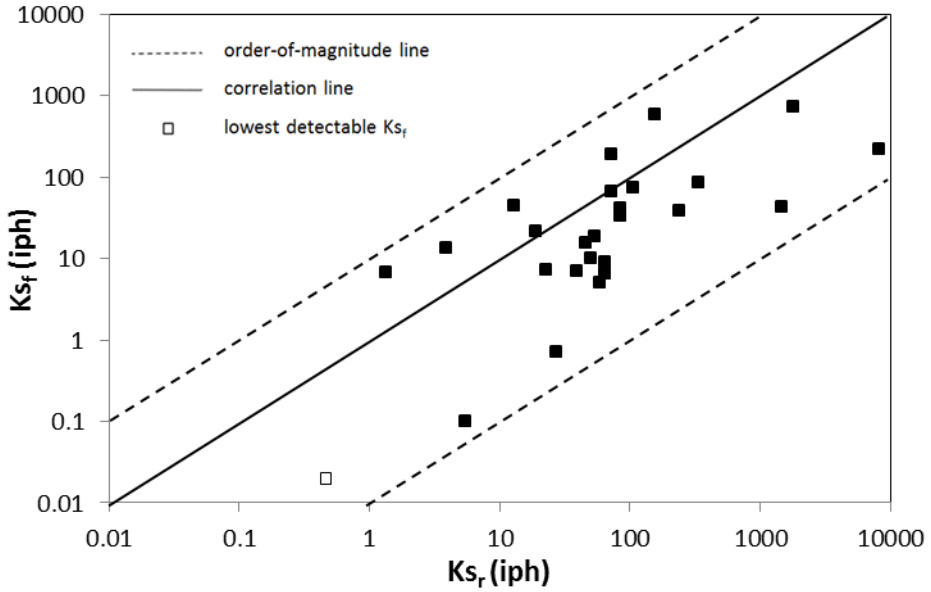

Figure 7. Equation 3 for normally consolidated samples (Qvr+Qal). Ks_f = field saturated hydraulic conductivity (iph) and Ks_r = saturated hydraulic conductivity from regression equations (iph).

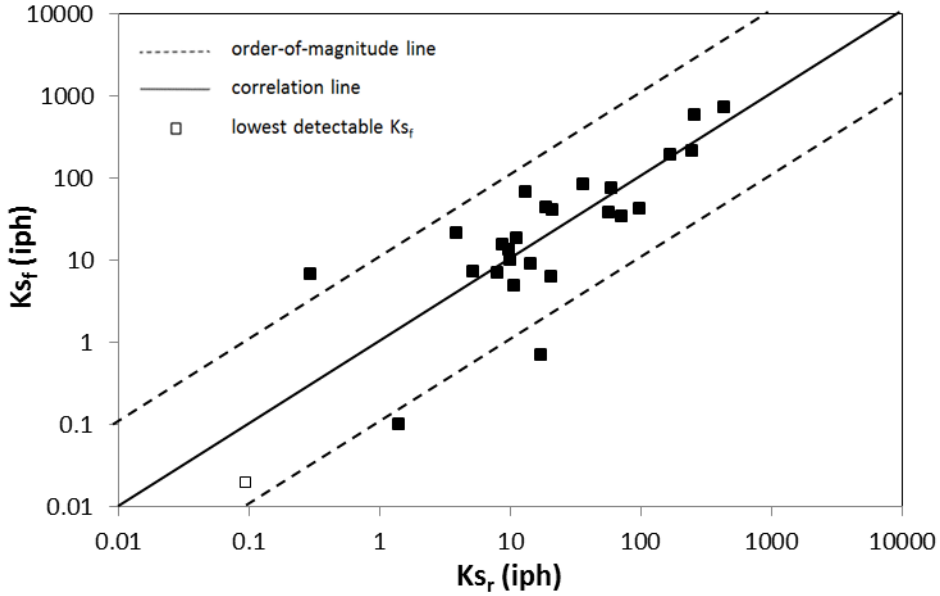

Figure 8. Equation B.1 for normally consolidated samples (Qvr+Qal). Ks_f = field saturated hydraulic conductivity (iph) and Ks_r = saturated hydraulic conductivity from regression equations (iph).

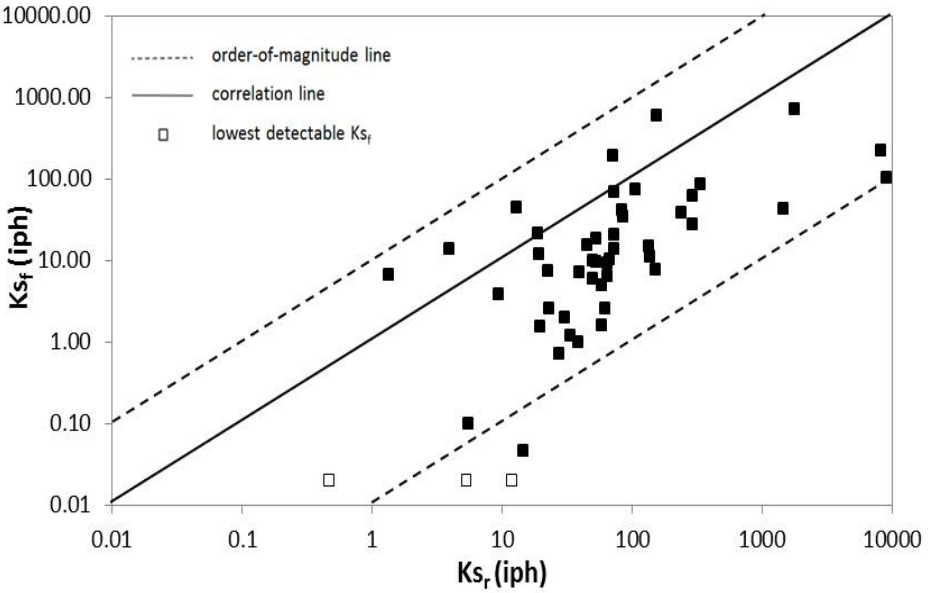

Figure 9. Equation 3 for mixed samples (Qva+Qvr+Qal). Ks_f = field saturated hydraulic conductivity (iph) and Ks_r = saturated hydraulic conductivity from regression equations (iph).

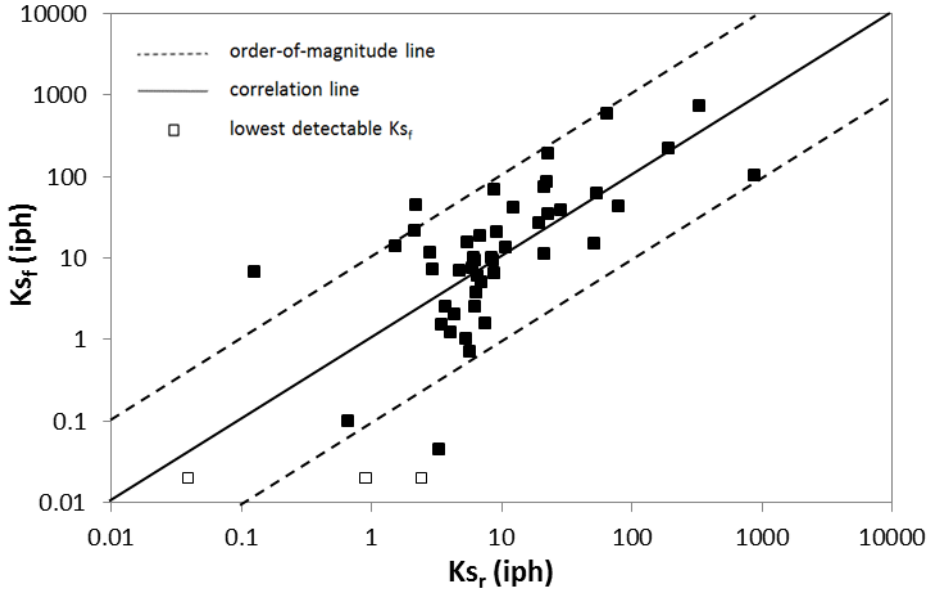

Figure 10. Equation C.1 for mixed samples (Qva+Qvr+Qal). Ks_f = field saturated hydraulic conductivity (iph) and Ks_r = saturated hydraulic conductivity from regression equations (iph).

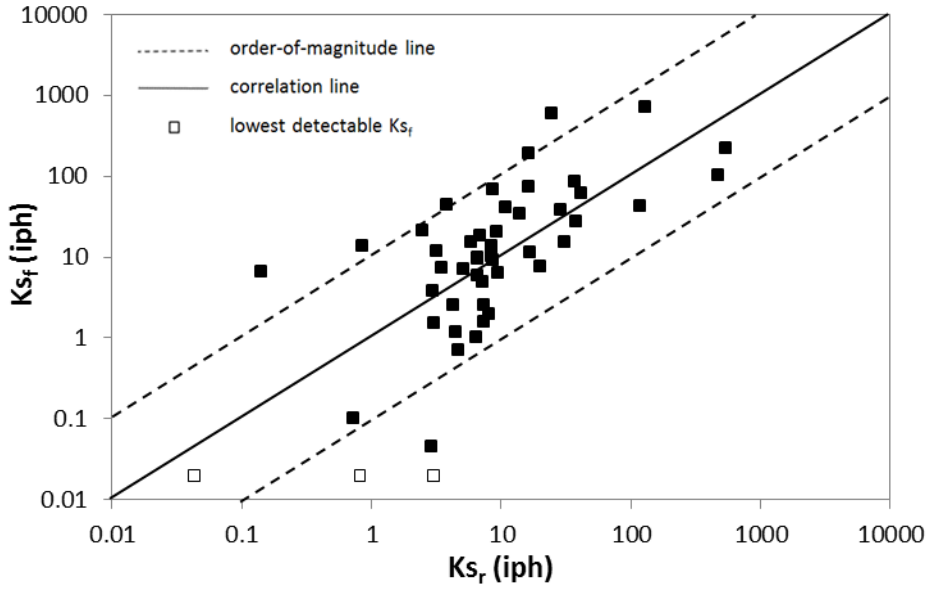

Figure 11. Equation C.2 for mixed samples (Qva+Qvr+Qal). Ks_f = field saturated hydraulic conductivity (iph) and Ks_r = saturated hydraulic conductivity from regression equations (iph).

Tables

Table 1. Geometric mean for observed data.

Data Set	Geometric Mean Ks_f (iph)
over consolidated	3
normally consolidated	17
mixed	8

*Ks_f = field saturated hydraulic conductivity (iph).

Table 2. Regression equations.

Eqn. A.1	$\log_{10}(Ks_r) = 0.99 + 1.47d_{10} - 0.071d_{60} + 0.010d_{90} - 8.31f_{fines}$
Eqn. A.2	$\log_{10}(Ks_r) = 0.88 + 1.01d_{10} - 7.59f_{fines}$
Eqn. B.1	$\log_{10}(Ks_r) = 0.91 + 1.63d_{10} - 0.12d_{60} + 0.048d_{90} - 2.12f_{fines}$
Eqn. C.1	$\log_{10}(Ks_r) = 0.67 + 2.00d_{10} - 0.075d_{60} + 0.018d_{90} - 2.29f_{fines}$
Eqn. C.2	$\log_{10}(Ks_r) = 0.75 + 1.46d_{10} - 2.32f_{fines}$
Eqn. 3	$\log_{10}(Ks_r) = -1.57 + 1.90d_{10} + 0.015d_{60} - 0.013d_{90} - 2.08f_{fines}$

*Ks_r = saturated hydraulic conductivity from regression equations (cm/s), d_{10}, d_{60}, and d_{90} are the grain sizes (mm) for which 10, 60 , and 90% of the material is more fine, and f_{fines} is the fraction of the material (by weight) that passes the number-200 sieve (0.075 mm). Equation 3 = Massmann's regression equation (Massmann, 2003).

Table 3. Statistical summary between regression equations and the population. Equations shown in Table 2.

Data Set	Analysis Method	Variance of $\log_{10}(Ks)$	σ	R^2
over consolidated	Population	0.93	9.2	-
normally consolidated	"	0.99	9.9	-
mixed	"	1.09	11	-
over consolidated	Eqn. 3	1.94	25	0.68
normally consolidated	"	0.76	7.4	0.15
mixed	"	1.32	14	0.12
over consolidated	Eqn. A.1	0.28	3.4	0.78
over consolidated	Eqn. A.2	0.32	3.7	0.85
normally consolidated	Eqn. B.1	0.31	3.6	0.90
mixed	Eqn. C.1	0.54	5.4	0.20
mixed	Eqn. C.2	0.58	5.8	0.16

*Ks = saturated hydraulic conductivity (iph) and σ = one standard deviation expressed as a multiplicative factor. R^2 = correlation coefficient.

Appendix A. Forty-nine pairs of grain-size and field-*Ks* data.

Layering?	City, WA	Unit	Soil Class	d_{10} (mm)	d_{60} (mm)	d_{90} (mm)	f_{fines}	Ks_f (iph)
N	Arlington	Qvr	SP	0.32	4.07	17.13	0.00	74.50
N	Auburn	Qal	SP	0.20	0.49	0.74	0.04	67.74
Y	Auburn	Qal	SP-SM	0.11	0.37	0.68	0.06	15.39
N	Auburn	Qal	SP-SM	0.03	0.39	0.70	0.11	7.28
N	Auburn	Qvr	SM	0.03	0.16	1.25	0.40	0.10
N	Bain Bridge Island	Qvr	SP	0.21	3.89	12.23	0.04	6.44
N	Bain Bridge Island	Qvr	SP-SM	0.16	0.48	0.75	0.05	4.99
N	Bellevue	Qvr	SP	0.21	0.55	3.33	0.01	41.10
N	Bellevue	Qvr	SP-SM	0.10	0.48	1.30	0.08	7.00
N	Black Diamond	Qvr	GW	1.39	27.55	51.57	0.02	217.80
N	Black Diamond	Qvr	SP	0.46	1.80	20.45	0.01	582.60
N	Issaquah	Qvr	GP	0.59	11.69	22.96	0.02	84.36
N	Issaquah	Qvr	GP-GM	0.06	12.75	41.41	0.11	43.99
N	Issaquah	Qvr	GW	0.39	9.32	38.86	0.05	193.41
N	Marysville	Qvr	SW-SM	0.09	0.79	9.89	0.09	0.70
N	North Bend	Qal	GW	0.51	7.29	18.65	0.01	38.00
N	North Bend	Qal	SM	0.00	0.02	0.61	0.69	6.70
N	North Bend	Qal	SM	0.04	0.33	0.81	0.18	21.46
N	Seattle	Qal	SM	0.01	0.04	0.07	0.92	0.02
N	Seattle	Qvr	SM	0.02	0.37	18.00	0.37	13.70
N	Seattle	Qvr	SP	0.11	0.28	0.75	0.04	10.00
N	Seattle	Qvr	SP	0.14	0.33	1.61	0.01	9.20
N	Seattle	Qvr	SP-SM	0.14	0.37	1.33	0.05	18.58
N	Snoqualmie	Qvr	SM	0.96	3.40	12.40	0.02	720.00
N	Tacoma	Qvr	GW	0.90	14.01	26.08	0.00	43.00
N	Woodinville	Qvr	SP	0.27	1.69	14.61	0.00	34.00
N	Black Diamond	Qva	GP	0.57	11.94	48.37	0.04	15.00
N	Bonney Lake	Qva	GP	0.18	14.42	42.98	0.05	2.00
N	Bonney Lake	Qva	GW	1.33	10.11	21.33	0.01	101.22
N	Fall City	Qva	GP	0.58	14.68	31.78	0.01	27.00
N	Issaquah	Qva	GP	0.62	9.56	31.22	0.02	60.91
N	Marysville	Qva	SP	0.17	0.58	1.52	0.03	10.08
N	Marysville	Qva	SP-SM	0.16	5.23	16.68	0.08	1.00
N	Redmond	Qva	SM	0.04	0.73	23.90	0.15	3.78
N	Seatac	Qva	GP	0.39	15.40	27.33	0.01	7.60
N	Seattle	Qva	SM	0.01	0.41	7.32	0.37	0.02
N	Seattle	Qva	SM	0.05	0.38	1.35	0.14	11.80
N	Seattle	Qva	SM	0.05	0.57	7.92	0.16	0.04

N	Seattle	Qva	SM	0.05	0.41	7.00	0.14	1.54
N	Seattle	Qva	SP	0.16	0.38	1.49	0.05	1.56
N	Seattle	Qva	SP	0.18	0.71	1.88	0.02	20.67
Y	Seattle	Qva	SP	0.18	1.29	10.00	0.04	13.58
Y	Seattle	Qva	SP	0.36	2.08	8.26	0.03	11.20
N	Seattle	Qva	SP-SM	0.08	0.67	1.56	0.10	2.56
N	Seattle	Qva	SP-SM	0.16	1.12	0.00	0.05	2.52
N	Seattle	Qva	SP-SM	0.14	0.39	1.84	0.06	5.94
Y	Seattle	Qva	SW-SM	0.08	0.64	1.79	0.09	1.20
Y	Seattle	Qva	GM	0.05	6.25	22.85	0.15	.02
N	Woodinville	Qva	SP-SM	0.15	0.50	0.77	0.07	9.40

*Layering = stratified layers of silt and clay (i.e. heterogeneous materials).

Appendix B. Data for grain-size distribution curve in Figure 3.

Mesh # =	**3"**	**2.5"**	**2"**	**1.5"**	**#4**	**#10**	**#40**	**#100**	**#200**	**#270**
Mesh Size (mm) =	**76.10**	**64.00**	**50.80**	**38.10**	**4.76**	**2.00**	**0.42**	**0.15**	**0.07**	**0.06**
Qva				100.00	39.69	25.15	7.15	2.17	1.14	0.94
Qva		100.00	90.70	86.60	41.20	30.40	7.70	5.30	4.40	
Qva				100.00	34.70	15.26	2.06	1.60	1.48	1.39
Qva				100.00	48.94	32.62	5.97	2.56	1.85	1.66
Qva				100.00	36.40	30.50	10.90	2.10	1.00	0.80
Qva				100	80.20	58.80	11.90	3.40	2.80	2.60
Qva				100	78.75	70.73	32.67	5.41	3.72	
Qva				100	96.23	91.95	44.00	3.70	1.98	1.81
Qva				100	99.84	98.65	49.83	4.88	3.10	2.90
Qva				100	81.08	72.85	38.41	7.91	5.14	
Qva				100	97.67	95.85	65.18	7.13	4.72	4.33
Qva				100	99.90	99.40	48.80	9.80	6.80	6.30
Qva				100	94.93	91.49	63.22	10.58	5.92	
Qva				100	57.50	44.30	23.70	9.40	7.60	7.20
Qva				100	99.03	93.25	47.84	13.09	9.47	
Qva	100.00	92.50	92.50	88.20	40.70	32.40	20.70	7.60	4.80	
Qva				100	99.38	98.88	43.27	12.37	10.11	
Qva				100	85.76	79.57	60.52	19.47	14.23	
Qva				100	96.30	92.50	66.70	18.90	13.70	12.70
Qva				100	85.00	78.70	51.30	23.00	15.70	13.60
Qva				100.00	72.50	68.10	48.20	23.30	14.70	12.60
Qva				100	87.20	79.20	60.70	42.80	37.00	35.40
Qva				100	56.70	50.20	35.30	18.70	14.70	13.70
Qal					100.00	99.96	49.74	5.35	4.24	4.12
Qal						100.00	70.04	12.96	6.18	5.63
Qal				100.00	45.87	28.24	6.49	1.47	1.23	
Qal					100.00	99.70	68.80	33.70	18.00	14.00
Qal					100.00	99.75	83.79	73.58	69.29	
Qal					100.00	99.98	65.55	12.05	10.77	10.73
Qal					100.00	99.87	99.62	96.94	91.99	84.02
Qvr				100.00	73.30	64.30	6.90	1.90	1.40	
Qvr		100.00	89.30	74.40	19.00	11.80	5.20	2.40	1.90	
Qvr				100	72.66	40.77	3.03	1.97	1.76	
Qvr				100.00	33.80	19.50	3.80	0.70	0.10	0.00
Qvr				100.00	40.44	28.17	6.37	2.58	1.85	1.66
Qvr				100.00	62.62	48.16	15.34	1.25	0.37	
Qvr				100.00	69.60	61.40	23.30	2.30	0.30	0.20
Qvr				100.00	91.90	87.00	47.20	3.20	0.60	0.50
Qvr			100.00	89.26	45.32	28.45	10.44	5.82	4.74	4.40
Qvr				100.00	93.10	90.90	75.10	10.70	1.10	0.60

Qvr				100.00	64.50	46.00	23.10	5.50	3.60	3.20
Qvr					100.00	99.60	51.30	8.90	5.20	4.60
Qvr				100	98.94	98.33	66.28	10.51	5.11	
Qvr				100.00	92.90	92.20	84.40	15.70	3.90	
Qvr				100.00	98.70	97.10	50.90	12.00	8.30	7.30
Qvr				100.00	84.90	77.70	32.40	12.60	9.20	
Qvr			100.00	85.92	43.32	31.97	20.06	14.54	10.99	9.72
Qvr				100.00	95.80	91.60	85.10	56.40	39.80	
Qvr				100	75.80	70.90	62.10	46.30	36.60	33.10

Appendix C. Equation A.1 regression data for over consolidated (Qva) samples.

Unit	d_{10} (mm)	d_{60} (mm)	d_{90} (mm)	f_{fines}	Ks_r (iph) Eqn. 3	Ks_f (iph)	Ks_r (iph) Eqn. A.1
Qva	0.01	0.41	7.32	0.37	5.28	0.02	0.01
Qva	0.05	6.25	22.85	0.15	11.81	0.02	0.43
Qva	0.05	0.57	7.92	0.16	14.47	0.04	0.63
Qva	0.05	0.38	1.35	0.14	19.26	11.80	0.80
Qva	0.05	0.41	7.00	0.14	19.57	1.54	0.82
Qva	0.04	0.73	23.90	0.15	9.46	3.78	1.05
Qva	0.08	0.67	1.56	0.10	22.96	2.56	1.68
Qva	0.18	14.42	42.98	0.05	30.64	2.00	1.93
Qva	0.08	0.64	1.79	0.09	33.61	1.20	1.96
Qva	0.16	5.23	16.68	0.08	38.59	1.00	2.47
Qva	0.15	0.50	0.77	0.07	52.91	9.40	4.12
Qva	0.39	15.40	27.33	0.01	150.75	7.60	4.71
Qva	0.14	0.39	1.84	0.06	50.09	5.94	4.85
Qva	0.16	1.12	0.00	0.05	62.42	2.52	5.18
Qva	0.16	0.38	1.49	0.05	58.57	1.56	6.49
Qva	0.17	0.58	1.52	0.03	66.76	10.08	8.89
Qva	0.18	1.29	10.00	0.04	72.51	13.58	8.92
Qva	0.58	14.68	31.78	0.01	293.08	27.00	10.91
Qva	0.18	0.71	1.88	0.02	72.33	20.67	11.17
Qva	0.57	11.94	48.37	0.04	135.00	15.00	13.33
Qva	0.36	2.08	8.26	0.03	137.13	11.20	16.81
Qva	0.62	9.56	31.22	0.02	292.44	60.91	25.08
Qva	1.33	10.11	21.33	0.01	9125.91	101.22	213.48

Appendix D. Equation A.2 regression data for over consolidated (Qva) samples.

Unit	d_{10} **(mm)**	f_{fines}	Ks_r **(iph) Eqn. 3**	Ks_f **(iph)**	Ks_r **(iph) Eqn. A.2**
Qva	0.01	0.37	5.28	0.02	0.01
Qva	0.05	0.15	11.81	0.02	0.65
Qva	0.05	0.16	14.47	0.04	0.55
Qva	0.05	0.14	19.26	11.80	0.77
Qva	0.05	0.14	19.57	1.54	0.71
Qva	0.04	0.15	9.46	3.78	0.64
Qva	0.08	0.10	22.96	2.56	1.56
Qva	0.18	0.05	30.64	2.00	5.06
Qva	0.08	0.09	33.61	1.20	1.77
Qva	0.16	0.08	38.59	1.00	2.93
Qva	0.15	0.07	52.91	9.40	3.31
Qva	0.39	0.01	150.75	7.60	15.99
Qva	0.14	0.06	50.09	5.94	3.74
Qva	0.16	0.05	62.42	2.52	4.53
Qva	0.16	0.05	58.57	1.56	4.83
Qva	0.17	0.03	66.76	10.08	6.58
Qva	0.18	0.04	72.51	13.58	6.04
Qva	0.58	0.01	293.08	27.00	24.30
Qva	0.18	0.02	72.33	20.67	8.14
Qva	0.57	0.04	135.00	15.00	13.54
Qva	0.36	0.03	137.13	11.20	10.95
Qva	0.62	0.02	292.44	60.91	23.79
Qva	1.33	0.01	9125.91	101.22	133.46

Appendix E. Equation B.1 regression data for normally con solidated (Qvr+Qal) samples.

Unit	d_{10} (mm)	d_{60} (mm)	d_{90} (mm)	f_{fines}	Ks_r (iph) Eqn. 3	Ks_f (iph)	Ks_r (iph) Eqn. B.1
Qal	0.01	0.04	0.07	0.92	0.46	0.02	0.09
Qal	0.00	0.02	0.61	0.69	1.36	6.70	0.30
Qvr	0.03	0.16	1.25	0.40	5.49	0.10	1.41
Qal	0.04	0.33	0.81	0.18	18.98	21.46	3.94
Qal	0.03	0.39	0.70	0.11	22.61	7.28	5.23
Qvr	0.10	0.48	1.30	0.08	39.17	7.00	8.10
Qal	0.11	0.37	0.68	0.06	45.53	15.39	8.88
Qvr	0.02	0.37	18.00	0.37	3.90	13.70	9.91
Qvr	0.11	0.28	0.75	0.04	49.77	10.00	10.13
Qvr	0.16	0.48	0.75	0.05	58.56	4.99	10.86
Qvr	0.14	0.37	1.33	0.05	53.50	18.58	11.24
Qal	0.20	0.49	0.74	0.04	72.89	67.74	13.16
Qvr	0.14	0.33	1.61	0.01	64.79	9.20	14.41
Qvr	0.09	0.79	9.89	0.09	27.49	0.70	17.52
Qvr	0.06	12.75	41.41	0.11	13.01	43.99	18.95
Qvr	0.21	3.89	12.23	0.04	64.40	6.44	20.68
Qvr	0.21	0.55	3.33	0.01	83.88	41.10	21.39
Qvr	0.59	11.69	22.96	0.02	339.94	84.36	36.84
Qal	0.51	7.29	18.65	0.01	242.28	38.00	57.33
Qvr	0.32	4.07	17.13	0.00	106.81	74.50	60.73
Qvr	0.27	1.69	14.61	0.00	85.47	34.00	72.73
Qvr	0.90	14.01	26.08	0.00	1455.93	43.00	99.68
Qvr	0.39	9.32	38.86	0.05	71.96	193.41	170.99
Qvr	1.39	27.55	51.57	0.02	8281.46	217.80	249.27
Qvr	0.46	1.80	20.45	0.01	155.36	582.60	259.87
Qvr	0.96	3.40	12.40	0.02	1799.47	720.00	436.81

Appendix F. Equation C.1 regression data for mixed samples.

Unit	d_{10} (mm)	d_{60} (mm)	d_{90} (mm)	f_{fines}	Ks_r (iph) Eqn. 3	Ks_f (iph)	Ks_r (iph) Eqn. C.1
Qva	1.33	10.11	21.33	0.01	9125.91	101.22	879.44
Qvr	1.39	27.55	51.57	0.02	8281.46	217.80	192.45
Qvr	0.96	3.40	12.40	0.02	1799.47	720.00	335.27
Qvr	0.90	14.01	26.08	0.00	1455.93	43.00	80.10
Qvr	0.59	11.69	22.96	0.02	339.94	84.36	22.26
Qva	0.58	14.68	31.78	0.01	293.08	27.00	19.56
Qva	0.62	9.56	31.22	0.02	292.44	60.91	54.65
Qal	0.51	7.29	18.65	0.01	242.28	38.00	28.51
Qal	0.46	1.80	20.45	0.01	155.36	582.60	64.38
Qva	0.39	15.40	27.33	0.01	150.75	7.60	6.00
Qva	0.36	2.08	8.26	0.03	137.13	11.20	21.53
Qva	0.57	11.94	48.37	0.04	135.00	15.00	51.85
Qvr	0.32	4.07	17.13	0.00	106.81	74.50	21.10
Qvr	0.27	1.69	14.61	0.00	85.47	34.00	22.85
Qvr	0.21	0.55	3.33	0.01	83.88	41.10	12.35
Qal	0.20	0.49	0.74	0.04	72.89	67.74	8.83
Qva	0.18	1.29	10.00	0.04	72.51	13.58	10.75
Qva	0.18	0.71	1.88	0.02	72.33	20.67	9.14
Qvr	0.39	9.32	38.86	0.05	71.96	193.41	22.91
Qva	0.17	0.58	1.52	0.03	66.76	10.08	8.38
Qvr	0.14	0.33	1.61	0.01	64.79	9.20	8.67
Qvr	0.21	3.89	12.23	0.04	64.40	6.44	8.89
Qva	0.16	1.12	0.00	0.05	62.42	2.52	6.21
Qva	0.16	0.38	1.49	0.05	58.57	1.56	7.56
Qvr	0.16	0.48	0.75	0.05	58.56	4.99	7.01
Qvr	0.14	0.37	1.33	0.05	53.50	18.58	6.81
Qva	0.15	0.50	0.77	0.07	52.91	9.40	6.27
Qva	0.14	0.39	1.84	0.06	50.09	5.94	6.55
Qvr	0.11	0.28	0.75	0.04	49.77	10.00	6.18
Qal	0.11	0.37	0.68	0.06	45.53	15.39	5.46
Qvr	0.10	0.48	1.30	0.08	39.17	7.00	4.75
Qva	0.16	5.23	16.68	0.08	38.59	1.00	5.39
Qva	0.08	0.64	1.79	0.09	33.61	1.20	4.04
Qva	0.18	14.42	42.98	0.05	30.64	2.00	4.34
Qvr	0.09	0.79	9.89	0.09	27.49	0.70	5.76
Qva	0.08	0.67	1.56	0.10	22.96	2.56	3.73
Qal	0.03	0.39	0.70	0.11	22.61	7.28	2.96
Qva	0.05	0.41	7.00	0.14	19.57	1.54	3.44

Qva	0.05	0.38	1.35	0.14	19.26	11.80	2.80
Qal	0.04	0.33	0.81	0.18	18.98	21.46	2.16
Qva	0.05	0.57	7.92	0.16	*14.47*	*0.04*	3.30
Qvr	0.06	12.75	41.41	0.11	13.01	43.99	2.19
Qva	0.05	6.25	22.85	0.15	11.81	0.02	2.39
Qva	0.04	0.73	23.90	0.15	9.46	3.78	6.35
Qvr	0.03	0.16	1.25	0.40	5.49	0.10	0.67
Qva	0.01	0.41	7.32	0.37	5.28	0.02	0.89
Qvr	0.02	0.37	18.00	0.37	3.90	13.70	1.52
Qal	0.00	0.02	0.61	0.69	1.36	6.70	0.13
Qal	0.01	0.04	0.07	0.92	0.46	0.02	0.04

Appendix G. Equation C.2 regression data for mixed (Qva+Qvr+Qal) samples.

Unit	d_{10} (mm)	f_{fines}	Ks_r (iph) Eqn. 3	Ks_f (iph)	Ks_r (iph) Eqn. C.2
Qva	1.33	0.01	9125.91	101.22	467.71
Qvr	1.39	0.02	8281.46	217.80	544.33
Qvr	0.96	0.02	1799.47	720.00	129.83
Qvr	0.90	0.00	1455.93	43.00	117.18
Qvr	0.59	0.02	339.94	84.36	36.78
Qva	0.58	0.01	293.08	27.00	37.57
Qva	0.62	0.02	292.44	60.91	41.94
Qal	0.51	0.01	242.28	38.00	29.14
Qal	0.46	0.01	155.36	582.60	24.90
Qva	0.39	0.01	150.75	7.60	19.99
Qva	0.36	0.03	137.13	11.20	16.56
Qva	0.57	0.04	135.00	15.00	30.89
Qvr	0.32	0.00	106.81	74.50	16.55
Qvr	0.27	0.00	85.47	34.00	14.03
Qvr	0.21	0.01	83.88	41.10	10.94
Qal	0.20	0.04	72.89	67.74	8.72
Qva	0.18	0.04	72.51	13.58	8.43
Qva	0.18	0.02	72.33	20.67	9.19
Qvr	0.39	0.05	71.96	193.41	16.30
Qva	0.17	0.03	66.76	10.08	8.44
Qvr	0.14	0.01	64.79	9.20	8.60
Qvr	0.21	0.04	64.40	6.44	9.54
Qva	0.16	0.05	62.42	2.52	7.37
Qva	0.16	0.05	58.57	1.56	7.46
Qvr	0.16	0.05	58.56	4.99	7.26
Qvr	0.14	0.05	53.50	18.58	6.89
Qva	0.15	0.07	52.91	9.40	6.54
Qva	0.14	0.06	50.09	5.94	6.54
Qvr	0.11	0.04	49.77	10.00	6.58
Qal	0.11	0.06	45.53	15.39	5.89
Qvr	0.10	0.08	39.17	7.00	5.12
Qva	0.16	0.08	38.59	1.00	6.44
Qva	0.08	0.09	33.61	1.20	4.50
Qva	0.18	0.05	30.64	2.00	8.10
Qvr	0.09	0.09	27.49	0.70	4.65
Qva	0.08	0.10	22.96	2.56	4.25
Qal	0.03	0.11	22.61	7.28	3.52
Qva	0.05	0.14	19.57	1.54	3.08
Qva	0.05	0.14	19.26	11.80	3.17
Qal	0.04	0.18	18.98	21.46	2.48

Qva	0.05	0.16	*14.47*	*0.04*	2.90
Qvr	0.06	0.11	13.01	43.99	3.81
Qva	0.05	0.15	11.81	0.02	3.00
Qva	0.04	0.15	9.46	3.78	2.95
Qvr	0.03	0.40	5.49	0.10	0.74
Qva	0.01	0.37	5.28	0.02	0.81
Qvr	0.02	0.37	3.90	13.70	0.86
Qal	0.00	0.69	1.36	6.70	0.14
Qal	0.01	0.92	0.46	0.02	0.04